Molecular Ferroelectricity

DOI: 10.1002/anie.201406810

An Above-Room-Temperature Ferroelectric Organo–Metal Halide Perovskite: (3-Pyrrolinium)($CdCl_3$)**

*Heng-Yun Ye, Yi Zhang, Da-Wei Fu, and Ren-Gen Xiong**

Abstract: *Hybrid organo–metal halide perovskite materials, such as $CH_3NH_3PbI_3$, have been shown to be some of the most competitive candidates for absorber materials in photovoltaic (PV) applications. However, their potential has not been completely developed, because a photovoltaic effect with an anomalously large voltage can be achieved only in a ferroelectric phase, while these materials are probably ferroelectric only at temperatures below 180 K. A new hexagonal stacking perovskite-type complex (3-pyrrolinium)($CdCl_3$) exhibits above-room-temperature ferroelectricity with a Curie temperature $T_c = 316$ K and a spontaneous polarization $P_s = 5.1\ \mu C\,cm^{-2}$. The material also exhibits antiparallel 180° domains which are related to the anomalous photovoltaic effect. The open-circuit photovoltage for a 1 mm-thick bulky crystal reaches 32 V. This finding could provide a new approach to develop solar cells based on organo–metal halide perovskites in photovoltaic research.*

Ferroelectric crystalline materials are characterized by a spontaneous polarization (P_s) that occurs below a Curie temperature (T_c) and can be switched using an external electric field.[1] It has been established that the switchable polarization is sensitive to external stimuli, such as stress, pressure, temperature, electric field, or chemical substances. Ferroelectric materials can also respond to light quanta to generate photocurrent, a phenomenon called the anomalous photovoltaic effect (APE).[1,2] Although the APE in ferroelectrics has been known for more than half a century, it has not been widely investigated.[2,3] With the ever-increasing global concern for clean and sustainable energy, there is now a renaissance in research on ferroelectric photovoltaics.[4] So far, research activities have focused mainly on the "bulk" photovoltaic effect in ferroelectric materials, although the underlying mechanism for this effect is not very clear.[1,5] The effect is believed to be associated with the loss of inversion symmetry in the distribution of defects, impurities, space charges, and polarizations in ferroelectrics. The APE in the typical ferroelectric compound $BiFeO_3$ originates from different domain walls and functions in a similar manner to that of a classical p–n junction, owing to the asymmetry in polarization.[6] The most significant difference between the photovoltaic effect in a ferroelectric material and in a conventional semiconductor p–n junction is the magnitude of the electric field that separates the photogenerated electron–hole pair; the effective electric field in a ferroelectric material is approximately one to two orders of magnitude higher than that in a p–n junction.

Hybrid organo–metal halide perovskite materials, such as $CH_3NH_3PbI_3$, have recently been shown to be some of the most competitive candidates for absorber materials in crystalline thin-film photovoltaic (PV) applications.[7,8] These materials offer significant advantages, such as an appropriate direct band gap, a high absorption coefficient and excellent carrier transport, as well as an apparent tolerance for defects. Hybrid perovskite solar cells have been reported with a remarkably high power conversion efficiency (PCE) of approximately 15% within the past several years.[7f] Moreover, the composition and structures of the low-cost hybrid perovskite materials can be easily tuned by adjusting the metal halide frameworks and the intercalated organic species. Nevertheless, the materials are not ferroelectric at room temperature (but are probably ferroelectric at temperatures below 180 K),[9] and thus lack the anomalously large photovoltage required for the process of converting solar light into electricity. It is predicted[10] that combining the ferroelectric APE with the advantages of hybrid perovskites would result in the formation of a new generation of PV solar cells which would be as cheap as fossil fuels. These systems would also have a higher PCE approaching those (up to 30%) measured for silicon or gallium arsenide solar cells.

To obtain a material with a synergetic combination of a large electron–hole diffusion length (greater than 1 micron) and a large photovoltage, an above-room-temperature organo–metal halide perovskite ferroelectric material is required. Although significant research has focused on designing organic–inorganic hybrid perovskite ferroelectrics,[11] relatively few ABX_3-type organo–metal halide perovskite ferroelectric materials are known (see Supporting Information for literature search details).[12] The characteristics of the ferroelectric domains of these systems, which are closely related to the APE, remain unexplored. In this context, we have synthesized a new hybrid perovskite ferroelectric compound (3-pyrrolinium)($CdCl_3$) (**1**) (Figure 1a) which displays an above-room-temperature Curie temperature $T_c = 316$ K, a large P_s value, and a low coercive field (E_c) as well as antiparallel 180° domains. To our knowledge, **1** is the first example of an organo–metal halide perovskite

[*] Dr. H.-Y. Ye, Dr. Y. Zhang, Dr. D.-W. Fu, Prof. R.-G. Xiong
Ordered Matter Science Research Center
Southeast University
Nanjing 211189 (P. R. China)
E-mail: xiongrg@seu.edu.cn

[**] This work was supported by 973 project (2014CB932103) and the National Natural Science Foundation of China (21290172, 91222101 and 21371032). X.R.G. sincerely thanks Professors Li Sheng-Hui, Chen Bin, and Yuan Guo-Liang for their help with the measurement of solid-state NMR experiments, APV effects, and PFM images, respectively.

Supporting information for this article is available on the WWW under http://dx.doi.org/10.1002/anie.201406810.

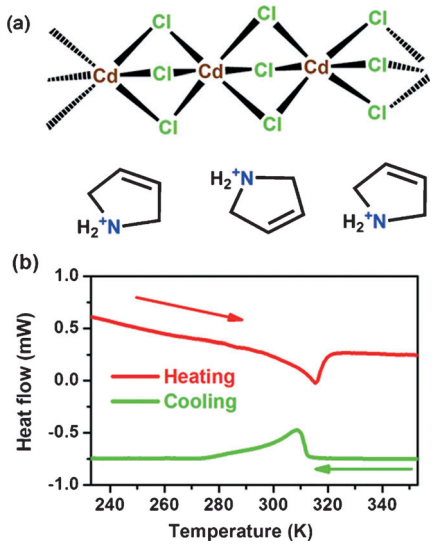

Figure 1. a) Chemical structures of the $(CdCl_3)_n$ chain and the intercalated 3-pyrrolinium cations in (3-pyrrolinium)$(CdCl_3)$ (**1**). b) DSC curves for polycrystalline samples of **1**, revealing a reversible phase transition at approximately 316 K.

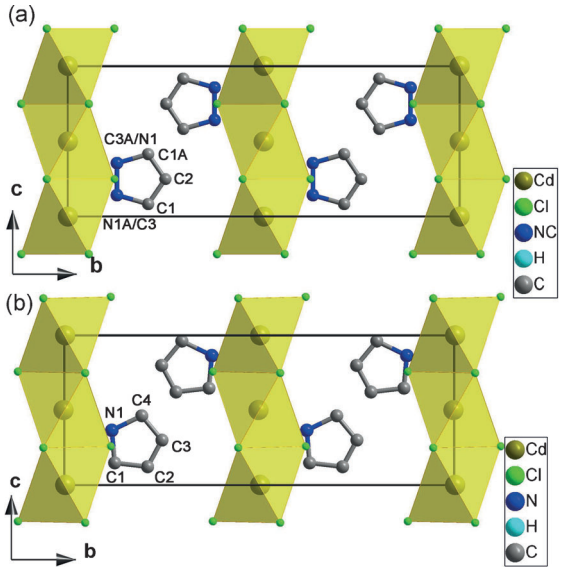

Figure 2. Packing views of **1** in a) the HTP and b) the LTP projected along the *a*-axis. The C and N atoms in a 3-pyrrolinium cation are labeled in both phases. In (a), the N1 and C3 sites are occupied equally by the C and N atoms. Atoms labelled with the suffix A are generated by symmetry operators. The hydrogen atoms of the organic cations were omitted for clarity.

ferroelectric material with an above-room-temperature T_c value, which allows us to investigate the APE of this class of materials. Herein, we describe the preparation of **1** and its excellent ferroelectric properties, domain structure, and APE.

We firstly performed differential scanning calorimetry (DSC) measurements to detect the structural phase transition in **1**. The DSC curves for polycrystalline samples of **1** showing cooling and heating runs are presented in Figure 1 b. The DSC result clearly shows that there is a reversible phase transition at around $T_c = 316$ K. The narrow thermal hysteresis (5 K) reveals a second-order transition. The thermal stability of **1** is maintained up to at least 573 K (see Figures S3 and S4 in the Supporting Information).

To understand the origin of the ferroelectric effect, a precise analysis of the main structural differences was undertaken between a series of structures of **1** determined by single-crystal X-ray diffraction at various temperatures.[13] The structure determined at 346 K is taken as the average structure of the high-temperature phase (HTP), and the structure at 293 K is taken as that of the low-temperature phase (LTP). The HTP crystallizes in the orthorhombic space group *Cmcm*. It has been shown that hybrid organic–inorganic perovskite ABX_3 materials can crystallize in two structural forms.[14] Firstly, materials such as $CH_3NH_3PbX_3$, $CH_3NH_3SnX_3$,[15] and the metal formate salts[11] may crystallize in a BX_6-corner-sharing cubic structure comparable to that of $BaTiO_3$. Alternatively, materials such as $N(CH_3)_4CdBr_3$[12a] may crystallize in a BX_6-face-sharing hexagonal structure comparable to that of $BaNiO_3$.[16] The crystal structure of compound **1** has a hexagonal perovskite-type structure and contains infinite columns of face-sharing $CdCl_6$ octahedra (Figure 2 and Figure S5 in the Supporting Information) which are arranged in the same manner as the NiO_6 moieties in the hexagonal 2-H $BaNiO_3$ structure.[16] The configuration of the chains are comparable to those in other ABX_3 compounds, such as $(CH_3)_4NCdCl_3$[17] and $[(CH_3)_3SO][CdCl_3]$.[18] The cavities between the octahedral columns are occupied by the 3-pyrrolinium cations, similar to the barium ions in the $BaNiO_3$ structure (Figure 2). The 3-pyrrolinium cation is located on a special position with $2mm$ symmetry. Although the 3-pyrrolinium cation has intermolecular $2mm$ symmetry with the N atom located on a twofold rotation axis, the intramolecular symmetry elements do not superimpose the crystallographic symmetry elements. The crystal symmetry requirement is satisfied by twofold orientational disorder with the C2 atom located on the crystallographic twofold axis, while the N atom is distributed equally over the mirror plane. As shown in Figure S5 a (Supporting Information), the elongated displacement ellipsoids of C1 and C2 atoms indicate the unresolved disorder and/or strong dynamics of the in-plane molecular rotation about the fixed N atom resulting from the N–H···Cl hydrogen-bonding interactions. Solid-state NMR spectra show that this effect is related to the in-plane swing-like motion about the N atom (see Supporting Information).

The LTP material crystallizes in the polar space group $Cmc2_1$. The coordination geometry of the Cd atom shows negligible change within the structure. Correspondingly, the off-center shift of the central Cd atom along the *c*-direction is 0.0094 Å. The cationic ring remains located on the mirror plane, while the mirror plane perpendicular to the ring plane is lost. The cationic ring was assigned and refined in a single orientation. However, the displacement ellipsoid of the C1 atom is obviously smaller than those for the other C atoms. The molecular geometry (indicated by examining the bond lengths: N1–C1 1.465(7), C1–C2 1.480(15), C2–C3 1.351(18), C3–C4 1.417(17), N1–C4 1.486(12) Å) points to

a somewhat disordered model. Additionally, the C3–C4 bond length becomes longer as the temperature decreases (Figure S6). These structural features indicate that as the crystal is cooled through the transition, it becomes only partly ordered and the long-range ordering takes place over a broad range of temperatures. This was further confirmed by solid-state NMR spectra (see Supporting Information). With the present ordered model, the average shift of the N atom along the *c*-axis is estimated to be 0.76 Å, much larger than the deviation of the Cd atom from the octahedron. This displacement may induce a polarization of approximately 5.6 $\mu C\,cm^{-2}$, slightly higher than the measured value $P_s = 5.1\ \mu C\,cm^{-2}$. This means that the P_s value derives mainly from the ordering of the organic cation. The structure is refined with a racemic twinning model, revealing the existence of 180° ferroelectric domains which is supported by piezoresponse force microscopy (PFM) imaging experiments (see below).

The ferroelectric nature of the transition is evident from the large dielectric constant anomalies at temperatures around the Curie temperature T_c. The temperature-dependent real part (ε') of the complex dielectric constant (defined as: $\varepsilon = \varepsilon' - i\varepsilon''$, where ε'' is the imaginary part) at each frequency (Figure 3) displays a pronounced λ-shape peak

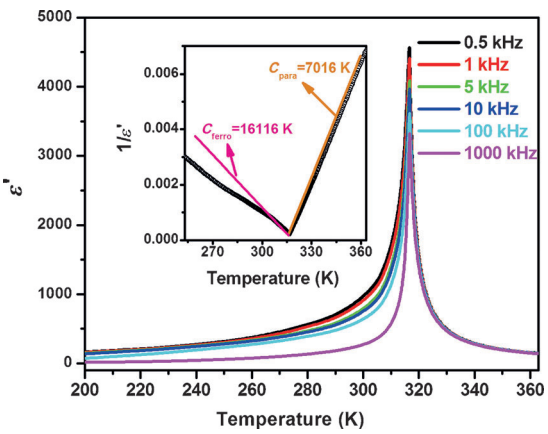

Figure 3. Temperature dependence of the real part ε' of the complex dielectric constant of **1**, measured along the *c*-axis. The complex electric permittivity is defined as $\varepsilon = \varepsilon' - i\varepsilon''$, where ε'' is the imaginary part. Inset: plot showing the reciprocal of ε' values at 500 Hz as a function of temperature.

around the T_c value. The large values for ε' of 4500–3000 indicate that **1** is a typical proper ferroelectric material. According to the Curie–Weiss law ($\varepsilon' = \varepsilon_0 + C_{para}/(T - T_0)$ or $\varepsilon' = C_{para}/(T - T_0)$ where ($T > T_c$) and $\varepsilon' = \varepsilon_0 + C_{ferro}/(T_0 - T)$ or $\varepsilon' = C_{ferro}/(T - T_0)$ ($T < T_c$), respectively), the reciprocal value of ε' as a function of temperature is linear. At 500 Hz, it follows the Curie–Weiss law very well at temperatures above T_c, while below T_c the law is followed only over a narrow temperature range. The intercept value T_0 (the Curie–Weiss temperature), obtained by extrapolation, is estimated to be 316 K, equal to T_c, suggesting that this phase transition is second-order, which is in good agreement with the DSC measurements. For a second-order ferroelectric transition, the ratio of Curie-–Weiss constants (C_{para}/C_{ferro}) falls in a range smaller than 4.[19a] In this case, the value of C_{para}/C_{ferro} is estimated to be 2.4, very close to the theoretical value of 2 expected for a second-order phase transition.[19b]

To further verify the ferroelectric effect, *P*–*E* hysteresis loops were measured, where *P* is the polarization and *E* is the electric field. As shown in Figure 4a, at 338 K a linear *P*–*E* curve is measured, revealing that the current state is

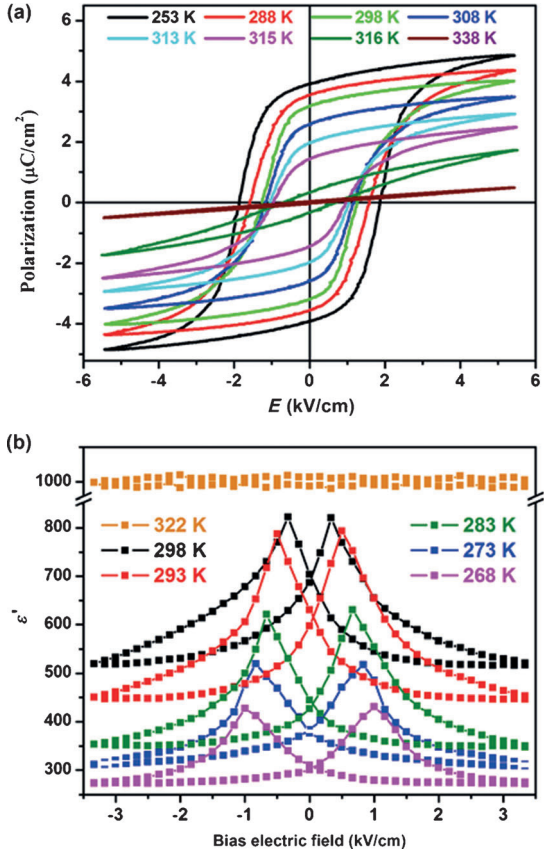

Figure 4. a) *P*–*E* hysteresis loops of **1** measured along the *c*-axis at various temperatures. b) Plot showing the dependence of the real part ε' of the complex dielectric constant of **1** on the bias electric field, measured along the *c*-axis at various temperatures.

a common paraelectric state. The *P*–*E* linear curve becomes a compressed S-shaped curve just below T_c, and then opens to form a loop upon further cooling, as is the characteristic feature of a ferroelectric. As the temperature decreases and the loop expands, the P_s value increases gradually, and reaches 5.1 $\mu C\,cm^{-2}$ with a remnant polarization (P_r) of 3.8 $\mu C\,cm^{-2}$ at 253 K. The P_s value measured at 253 K is larger than those found for $N(CH_3)_4CdBr_3$ (0.12 $\mu C\,cm^{-2}$),[12a] $(C_5H_9NH_3)(CdCl_3)$ (1.7 $\mu C\,cm^{-2}$),[12b] and metal formate perovskites with general formula $[NH_4][M(HCOO)_3]$ (0.97–2.2 $\mu C\,cm^{-2}$; where M = Zn, Mn, Co, Fe, Ni, Zn).[11b,d] The P_s value is also larger than some recently reported small-molecule organic ferroelectrics (1.2, 0.1, and 1.1 $\mu C\,cm^{-2}$ in [H-55DMBP][Hia],[20a] $[H_2\text{-TPPZ}][Hba]_2$,[20b] and Phz-H2ca,[20c] respectively), but smaller than those of several of the organic ferroelectrics (5.2, 22, 7, 55, and 23 $\mu C\,cm^{-2}$ in

MBI,[20d] croconic acid,[20e] α-[H-6,6′-dmbp][Hca],[20f] DHTTF-PMDI,[20g] and DIPAB,[20h] respectively). The relatively low operation voltage is evident from the small coercive field E_c in the range 1–2 kV cm^{-1}. The E_c value is lower than those measured for most of the small-molecule organic ferroelectrics and the metal–organic ferroelectrics,[11,12] and is three orders of magnitude lower than those measured for polymer ferroelectrics.[21] Below 253 K, the E_c value starts to increase rapidly without significant increases in P_r and P_s, indicating that the long-range ordering of the cations is almost complete.

The bias field dependence of the dielectric constant provides further evidence for reversible polarization switching. Figure 4b shows butterfly-shaped curves for the dependence of the ε' value on the bias voltage at temperatures below the Curie temperature T_c. With the changing voltage, peaking of the ε' value for each run shows hysteresis, similar to the hysteretic behavior measured in the P–E curve. Above T_c, the ε' value is independent of the bias field, consistent with the behavior of a paraelectric material.

The appearance of spontaneous polarization P_s was further confirmed by pyroelectric measurements. P_s, derived by integrating the pyroelectric current in a cooling run, appears at the Curie temperature T_c and then gradually increases with decreasing temperature (Figure 5). The gradual (not step-like) change near T_c suggests that the phase transition is of second-order. The P_s value is as large as 2.8–5.1 μC cm^{-2} in the temperature range from room temperature to 255 K, and reaches a maximum value at the lowest temperature. Both the P–E hysteresis and pyroelectricity support the above-room-temperature ferroelectricity in **1**.

Accompanying the paraelectric-to-ferroelectric phase transition, there should be a symmetry-breaking process in the crystal. In this case, this process involves a centrosymmetric-to-noncentrosymmetric transition. The loss of the inversion center was confirmed by measuring the variable-temperature second-order nonlinear optical coefficient ($\chi^{(2)}$; Figure 5). As expected, above the T_c, $\chi^{(2)}$ is almost zero; below T_c, it gradually increases to a detectable value. The gradual increase trend indicates a second-order transition. According to the Landau phenomenological theory, the two curves of the temperature-dependent normalized P_s value and $\chi^{(2)}$ should be overlapped. This is indeed the case in Figure 5, indicating that **1** is a typical proper ferroelectric, comparable to $BaTiO_3$.

Macroscopic evidence for the polarization switching is provided by an examination of the ferroelectric domains in a crystal of **1** along the *c*-axis by piezoresponse force microscopy (PFM) imaging. PFM is a powerful technique to probe the nucleation, growth, and switching of nanoscale ferroelectric domains. The amplitude of the detected piezoelectric vibration is a direct measurement of the piezoelectric coefficient of a crystal face, whereas the phase signal represents the polarization direction. The topology of the (0 0 1) face and the domain structure are presented in Figures 6a and b. Formation of electric domains is a signature of the appearance of spontaneous polarization P_s. The stripe-like domain structure is typical of an *mmmFmm*2 ferroelectric, whose ferroelectric domains should have the *mmm* symmetry of its prototype, as measured in Rochelle salt.

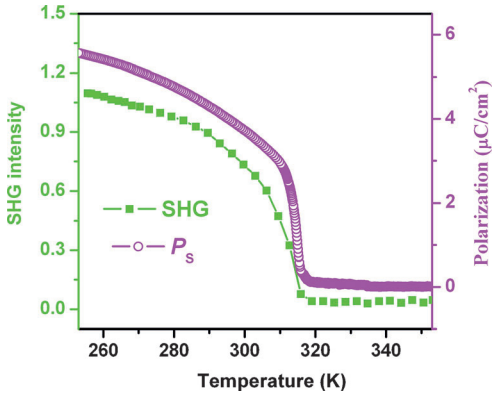

Figure 5. The temperature dependence of spontaneous polarization (P_s; pink), measured by integrating the pyroelectric current along the *c*-axis, and the second-order nonlinear optical coefficient ($\chi^{(2)}$; green) measured on polycrystals of **1**.

The characteristic feature of ferroelectric materials is the existence of switchable P_s values. To check the effect of the applied bias on the domain switching, an increasing bias of about ±40–50 V was applied to a (0 0 1) crystal face. The remnant phase and piezoelectric switching hysteresis measured at two spots are shown in Figures 6c and d, respectively. The amplitude shows a butterfly-like curve comparable to that measured for the bias-dependent ε' value, revealing the

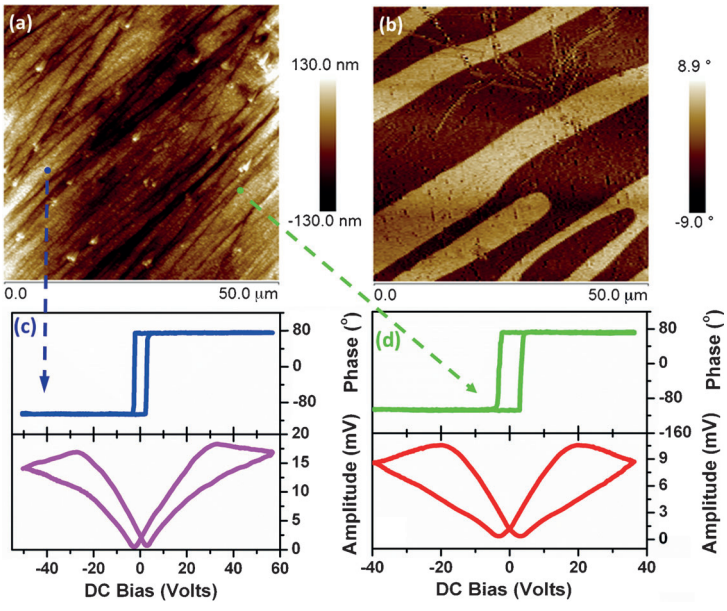

Figure 6. a) Topology image of the crystal face (0 0 1) of **1**. b) PFM image of a polarization pattern produced by applying a scanning voltage of 3.0 V using the tip. The brown-stripe regions correspond to downward polarization, while pale-yellow regions indicate upward polarization. c), d) Phase signal (top) and amplitude signal (bottom) plotted against DC bias, show local PFM hysteresis loops measured on the bulk crystal face (0 0 1) at two spots (indicated by the blue and green dashed arrows).

switching of the electric domains. The square-shaped phase hysteresis loop reveals a 180° domain reversal, further verifying the ability of the spontaneous polarization P_s to switch. The formation of 180° anti-parallel domains along $+z$ and $-z$ directions decreases the depolarizing field, which decreases the fatigue of the switching operation. This seems to be superior to that measured in ceramic perovskite ferroelectrics, such as $BaTiO_3$ and PTZ (which have 90° domains). In an ABO_3 perovskite ferroelectric, the off-center shift of the B atom causes a polarity change in the whole lattice, and correspondingly, polarization switching is realized through a displacement mechanism. In contrast, the off-center shift of the Cd atom in this case contributes little to P_s. P_s is derived mainly from the order–disorder transition of the organic 3-pyrrolinium cation. Accordingly, the polarization switching is achieved by the reorientation of the organic cation.[19]

In summary, by deliberate selection of organic cations, we have successfully designed a hybrid organo–metal halide perovskite (3-pyrrolinium)($CdCl_3$) which undergoes a phase transition at $T_c = 316$ K and has polarization and amplitude switching hystereses as well as 180° antiparallel domains. In combination, these features demonstrate that (3-pyrrolinium)($CdCl_3$) is an above-room-temperature organo–metal halide perovskite-like ferroelectric. The excellent above-room-temperature ferroelectric properties may find application in the electronic and/or optical fields. Moreover, the material shows an anomalous photovoltaic effect (Figure 7; see the Supporting Information for further details), as observed in $BiFeO_3$. The open-circuit photovoltage for a 1 mm-thick bulky crystal of **1** reaches about 32 V, much larger than that for the $CH_3NH_3PbI_3$ thin film (less than 1 V). These results may provide a new approach to develop solar cells based on organo–metal halide perovskites in photovoltaic research.

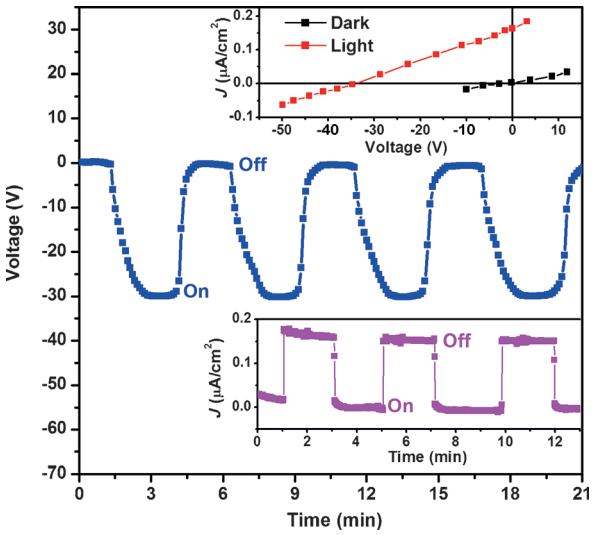

Figure 7. Short-circuit current (bottom) and open-circuit voltage (middle) versus measuring time for the ITO/(3-pyrrolinium)($CdCl_3$)-crystal/Ag-glue. Top: *J*–*V* characteristics for ITO/(3-pyrrolinium)($CdCl_3$)-crystal/Ag-glue capacitor in darkness and under illumination.

Experimental Section

All reagents were analytical grade and used without further purification. 3-pyrrolinium chloride was purchased from Jingyan Chemical Co., Ltd. (Shanghai, China), other reagents were purchased from Aladdin Chemistry Co., Ltd. (Shanghai, China). Distilled water is prepared in our lab. (3-Pyrrolinium)($CdCl_3$) (**1**) was obtained by slow evaporation of a clear aqueous solution ($\approx$130 mL) containing equal molar amounts of $CdCl_2$ (200 mmol) and 3-pyrrolinium chloride (200 mmol) at room temperature. Crystals up to 0.5 cm in size were formed after 3 weeks. Yield: >90%. FTIR: $\nu = 3150$ (m, $\nu_{N\text{-}H}$); 1620 (s; $\nu_{C=C}$) cm^{-1} (Figure S1). The purity of the bulk phase was verified by powder X-ray diffraction (PXRD; Figure S2).

CCDC 999019, 999020, 999021, 999022, 999023, 999024, 999025 contains the supplementary crystallographic data for this paper. These data can be obtained free of charge from The Cambridge Crystallographic Data Centre via www.ccdc.cam.ac.uk/data_request/cif.

Received: July 2, 2014
Revised: August 11, 2014
Published online: September 2, 2014

Keywords: domains · ferroelectrics · perovskites · phase transitions · polarization switching

[1] M. E. Lines, A. M. Glass, *Principles and Application of Ferroelectrics and Related Materials*, Oxford University Press, Oxford, **1977**.
[2] Y. Inoue, K. Sato, K. Sato, H. Miyama, *J. Phys. Chem.* **1986**, *90*, 2809–2810.
[3] a) A. Lempicki, *Phys. Rev.* **1959**, *113*, 1204–1209; b) L. Pensak, *Phys. Rev.* **1958**, *109*, 601; c) P. S. Brody, *Solid State Commun.* **1973**, *12*, 673–676.
[4] a) J. Kreisel, M. Alexe, P. A. Thomas, *Nat. Mater.* **2012**, *11*, 260; b) S. Y. Yang, J. Seidel, S. J. Byrnes, P. Shafer, C. H. Yang, M. D. Rossell, P. Yu, Y. H. Chu, J. F. Scott, J. W. Ager, L. W. Martin, R. Ramesh, *Nat. Nanotechnol.* **2010**, *5*, 143–147; c) M. Alexe, D. Hesse, *Nat. Commun.* **2011**, *2*, 256.
[5] a) A. M. Glass, D. von der Linde, T. J. Negran, *Appl. Phys. Lett.* **1974**, *25*, 233–235; b) A. M. Glass, D. von der Linde, D. H. Auston, T. J. Negran, *J. Electron. Mater.* **1975**, *4*, 915–943; c) P. S. Brody, F. Crowne, *J. Electron. Mater.* **1975**, *4*, 955–971; d) V. M. Fridkin, B. N. Popov, *Sov. Phys. Usp.* **1978**, *21*, 981–991.
[6] S. Y. Yang, L. W. Martin, S. J. Byrnes, T. E. Conry, S. R. Basu, D. Paran, L. Reichertz, J. Ihlefeld, C. Adamo, A. Melville, Y. H. Chu, C. H. Yang, J. L. Musfeldt, D. G. Schlom, J. W. Ager, R. Ramesh, *Appl. Phys. Lett.* **2009**, *95*, 062909.
[7] a) M. M. Lee, J. Teuscher, T. Miyasaka, T. N. Murakami, H. J. Snaith, *Science* **2012**, *338*, 643–647; b) D. J. Norris, E. S. Aydil, *Science* **2013**, *338*, 625–626; c) S. D. Stranks, G. E. Eperon, G. Grancini, C. Menelaou, M. J. P. Alcocer, T. Leijtens, L. M. Herz, A. Petrozza, H. J. Snaith, *Science* **2013**, *342*, 341–344; d) G. Xing, N. Mathews, S. Sun, S. S. Lim, Y. M. Lam, M. Grätzel, S. Mhaisalkar, T. C. Sum, *Science* **2013**, *342*, 344–347; e) M. Z. Liu, M. B. Johnston, H. J. Snaith, *Nature* **2013**, *501*, 395–398; f) J. Burschka, N. Pellet, S.-J. Moon, R. Humphry-Baker, P. Gao, M. K. Nazeeruddin, M. Grätzel, *Nature* **2013**, *499*, 316–319.
[8] a) M. A. Loi, J. C. Hummelen, *Nat. Mater.* **2013**, *12*, 1087–1089; b) P. V. Kamat, *J. Am. Chem. Soc.* **2014**, *136*, 3713–3714; c) L. Etgar, P. Gao, Z.-S. Xue, Q. Peng, A. K. Chandiran, B. Liu, M. K. Nazeeruddin, M. Grätzel, *J. Am. Chem. Soc.* **2012**, *134*, 17396–17399; d) L. C. Schmidt, A. Pertegás, S. González-Carrero, O. Malinkiewicz, S. Agouram, G. M. Espallargas, H. J. Bolink, R. E. Galian, J. Pérez-Prieto, *J. Am. Chem. Soc.* **2014**, *136*, 850–853; e) J. A. Christians, R. C. M. Fung, P. V. Kamat, *J. Am. Chem.*

Soc. **2014**, *136*, 758 – 764; f) N. Pellet, P. Gao, G. Gregori, T.-Y. Yang, M. K. Nazeeruddin, J. Maier, M. Grätzel, *Angew. Chem. Int. Ed.* **2014**, *53*, 3151 – 3157; *Angew. Chem.* **2014**, *126*, 3215 – 3221; g) B. V. Lotsch, *Angew. Chem. Int. Ed.* **2014**, *53*, 635 – 637; *Angew. Chem.* **2014**, *126*, 647 – 649; h) S. Kazim, M. K. Nazeeruddin, M. Grätzel, S. Ahmad, *Angew. Chem. Int. Ed.* **2014**, *53*, 2812 – 2824; *Angew. Chem.* **2014**, *126*, 2854 – 2867; i) B. Conings, L. Baeten, C. D. Dobbelaere, J. D'Haen, J. Manca, H.-G. Boyen, *Adv. Mater.* **2014**, *26*, 2041 – 2046; j) J.-Y. Jeng, Y.-F. Chiang, M.-H. Lee, S.-R. Peng, T.-F. Guo, P. Chen, T.-C. Wen, *Adv. Mater.* **2013**, *25*, 3727 – 3732; k) C. Wehrenfennig, G. E. Eperon, M. B. Johnston, H. J. Snaith, L. M. Herz, *Adv. Mater.* **2014**, *26*, 1584 – 1589.

[9] N. Onodayamamuro, T. Matsuo, H. Suga, *J. Phys. Chem. Solids* **1992**, *53*, 935 – 939.

[10] J. M. Frost, K. T. Butler, F. Brivio, C. H. Hendon, M. van Schilfgaarde, A. Walsh, *Nano Lett.* **2014**, *14*, 2584 – 2590.

[11] a) D. Di Sante, A. Stroppa, P. Jain, S. Picozzi, *J. Am. Chem. Soc.* **2013**, *135*, 18126 – 18130; b) G.-C. Xu, X.-M. Ma, L. Zhang, Z.-M. Wang, S. Gao, *J. Am. Chem. Soc.* **2010**, *132*, 9588 – 9592; c) P. Jain, V. Ramachandran, R. J. Clark, H. D. Zhou, B. H. Toby, N. S. Dalal, H. W. Kroto, A. K. Cheetham, *J. Am. Chem. Soc.* **2009**, *131*, 13625 – 13627; d) G.-C. Xu, W. Zhang, X.-M. Ma, Y.-H. Chen, L. Zhang, H.-L. Cai, Z.-M. Wang, R.-G. Xiong, S. Gao, *J. Am. Chem. Soc.* **2011**, *133*, 14948 – 14951; e) D.-W. Fu, W. Zhang, H.-L. Cai, Y. Zhang, J.-Z. Ge, R.-G. Xiong, *Angew. Chem. Int. Ed.* **2011**, *50*, 11947 – 11951; *Angew. Chem.* **2011**, *123*, 12153 – 12157; f) W. Zhang, R.-G. Xiong, *Chem. Rev.* **2012**, *112*, 1163 – 1195.

[12] a) K. Gesi, *J. Phys. Soc. Jpn.* **1990**, *59*, 432 – 434; b) Y. Zhang, H.-Y. Ye, W. Zhang, R.-G. Xiong, *Inorg. Chem. Front.* **2014**, *1*, 118 – 123.

[13] Crystal data for **1** at 346 K: $(C_4H_8N)(CdCl_3)$, $M_r = 288.86$, orthorhombic, *Cmcm*, $a = 7.434(4)$, $b = 17.441(9)$, $c = 6.707(3)$ Å, $V = 869.6(7)$ Å^3, $Z = 4$, $\rho_{cald} = 2.206$ g cm^{-3}, R_1 ($I > 2\sigma(I)$) = 0.0237, wR_2 (all data) = 0.0616, $m = 3.351$ mm^{-1}, $S = 1.144$. At 293 K: orthorhombic, $Cmc2_1$, $a = 7.446(17)$, $b = 17.43(4)$, $c = 6.764(15)$ Å, $V = 878(3)$ Å^3, $Z = 4$, $\rho_{cald} = 2.185$ g cm^{-3}, R_1 ($I > 2\sigma(I)$) = 0.0383, wR_2 (all data) = 0.0961, $m = 3.318$ mm^{-1}, $S = 1.089$. At 273 K: orthorhombic, $Cmc2_1$, $a = 7.402(7)$, $b = 17.383(16)$, $c = 6.699(7)$ Å, $V = 861.9(14)$ Å^3, $Z = 4$, $\rho_{cald} = 2.226$ g cm^{-3}, R_1 ($I > 2\sigma(I)$) = 0.0245, $wR2$ (all data) = 0.0959, $m = 3.881$ mm^{-1}, $S = 1.117$. At 253 K: orthorhombic, $Cmc2_1$, $a = 7.387(7)$, $b = 17.352(16)$, $c = 6.688(7)$ Å, $V = 857.2(14)$ Å^3, $Z = 4$, $\rho_{cald} = 2.238$ g cm^{-3}, R_1 ($I > 2\sigma(I)$) = 0.0195, wR_2 (all data) = 0.05, $m = 3.399$ mm^{-1}, $S = 1.053$. At 233 K: orthorhombic, $Cmc2_1$, $a = 7.381(7)$, $b = 17.340(17)$, $c = 6.686(7)$ Å, $V = 855.7(15)$ Å^3, $Z = 4$, $\rho_{cald} = 2.242$ g cm^{-3}, R_1 ($I > 2\sigma(I)$) = 0.0248, wR_2 (all data) = 0.0635, $m = 3.405$ mm^{-1}, $S = 1.084$. At 213 K: orthorhombic, $Cmc2_1$, $a = 7.367(6)$, $b = 17.319(13)$, $c = 6.678(5)$ Å, $V = 852.0(12)$ Å^3, $Z = 4$, $\rho_{cald} = 2.252$ g cm^{-3}, R_1 ($I > 2\sigma(I)$) = 0.0196, wR_2 (all data) = 0.0384, $m = 3.420$ mm^{-1}, $S = 1.003$. At 193 K: orthorhombic, $Cmc2_1$, $a = 7.366(7)$, $b = 17.313(16)$, $c = 6.679(7)$ Å, $V = 851.7(14)$ Å^3, $Z = 4$, $\rho_{cald} = 2.253$ g cm^{-3}, R_1 ($I > 2\sigma(I)$) = 0.0193, wR_2 (all data) = 0.0412, $m = 3.421$ mm^{-1}, $S = 1.021$.

[14] a) L. Katz, R. Ward, *Inorg. Chem.* **1964**, *3*, 205 – 211; b) J. Darriet, M. A. Subramanian, *J. Mater. Chem.* **1995**, *5*, 543 – 552.

[15] a) N. Onoda-Yamamuro, T. Matsuo, H. Suga, *J. Chem. Thermodyn.* **1991**, *23*, 987 – 999; b) K. Yamada, Y. Kuranaga, K. Ueda, S. Goto, T. Okuda, Y. Furrakawa, *Bull. Chem. Soc. Jpn.* **1998**, *71*, 127 – 134; c) Y. Takahashi, R. Obara, Z.-Z. Lin, Y. Takahashi, T. Naito, T. Inabe, S. Ishibashi, K. Terakura, *Discuss. Faraday Soc.* **2011**, *40*, 5563 – 5568.

[16] J. J. Lander, *Acta Crystallogr.* **1951**, *4*, 148 – 156.

[17] B. Morosin, *Acta Crystallogr. Sect. B* **1972**, *28*, 2303 – 2305.

[18] R. Puget, M. Jannin, C. D. Brauer, R. Perret, *Acta Crystallogr. Sect. C* **1991**, *47*, 1803 – 1805.

[19] a) D. A. Draegert, S. Singh, *Solid State Commun.* **1971**, *9*, 595 – 597; b) *Physics of Ferroelectrics—A Modern Perspective*, (Eds.: K. M. Rabe, C. H. Ahn, J.-M. Triscone), Springer, Berlin, **2007**.

[20] a) S. Horiuchi, R. Kumai, Y. Tokura, *Angew. Chem. Int. Ed.* **2007**, *46*, 3497 – 3501; *Angew. Chem.* **2007**, *119*, 3567 – 3571; b) S. Horiuchi, R. Kumai, Y. Tokunaga, Y. Tokura, *J. Am. Chem. Soc.* **2008**, *130*, 13382 – 13391; c) S. Horiuchi, F. Ishii, R. Kumai, Y. Okimoto, H. Tachibana, N. Nagaosa, Y. Tokura, *Nat. Mater.* **2005**, *4*, 163 – 166; d) S. Horiuchi, F. Kagawa, K. Hatahara, K. Kobayashi, R. Kumai, Y. Murakami, Y. Tokura, *Nat. Commun.* **2012**, *3*, 1308; e) S. Horiuchi, S. Tokunaga, G. Giovannetti, S. Picozzi, H. Itoh, R. Shimano, R. Kumai, Y. Tokura, *Nature* **2010**, *463*, 789 – 793; f) F. Kagawa, S. Horiuchi, N. Minami, S. Ishibashi, K. Kobayashi, R. Kumai, Y. Murakami, Y. Tokura, *Nano Lett.* **2014**, *14*, 239 – 243; g) A. S. Tayi, A. K. Shveyd, A. C.-H. Sue, J. M. Szarko, B. S. Rolczynski, D. Cao, T. Jackson Kennedy, A. A. Sarjeant, C. L. Stern, W. F. Paxton, W. Wu, S. K. Dey, A. C. Fahrenbach, J. R. Guest, H. Mohseni, L. X. Chen, K. L. Wang, J. F. Stoddart, S. I. Stupp, *Nature* **2012**, *488*, 485 – 489; h) D.-W. Fu, H.-L. Cai, Y. M. Liu, Q. Ye, W. Zhang, Y. Zhang, X.-Y. Chen, G. Giovannetti, M. Capone, J. Y. Li, R.-G. Xiong, *Science* **2013**, *339*, 425 – 428.

[21] T. Furukawa, *Phase Transitions* **1989**, *18*, 143 – 211.

